Observation of nonthermal turbulent electric fields in a nanosecond plasma opening switch experiment

A. Weingarten, S. Alexiou, Y. Maron, M. Sarfaty, and Ya. E. Krasik
Faculty of Physics, Weizmann Institute of Science, Rehovot 76100, Israel

A. S. Kingsep
Russian Research Center ''Kurchatov Institute,'' Kurchatov Square, 123182 Moscow, Russia
(Received 15 December 1997)

Nonthermal turbulent electric fields due to plasma instabilities were studied in a 100-ns duration plasma opening switch using observations of hydrogen line spectral profiles. The H_α and H_β widths were seen to rise by 2–3 times during the current pulse, shown to result from the presence of nonthermal electric fields in the plasma. The spectral profiles are analyzed using two recently developed methods based on short and intermediate time behaviors of the line profile Fourier transforms. One method gives the mean amplitude of the nonthermal fields with no dependence on their frequencies. The second method uses calculations of the autocorrelation functions for various field amplitudes and frequencies to yield bounds on these two parameters. The field amplitude is determined to be 14.5 ± 2.5 kV/cm, and the fluctuation frequency is found to be of the order of the electron plasma frequency. Based on their high frequency, the oscillations probably result from Langmuir waves, driven by the voltage drop on the plasma opening switch (POS). The waves have no significant effect on the POS operation, since they do not give rise to anomalous resistivity, and therefore have no effect on the magnetic-field evolution. We obtain an upper limit for the amplitude of possible low-frequency fields (ion-acoustic waves), that may give rise to anomalous resistivity, and estimate the resulting diffusion velocity and current channel width. Both quantities are found to be much lower than the values observed in the experiment, and the low-frequency field amplitude is much lower than the saturation limit predicted by previous theoretical treatments. This implies that in our experiment possible low-frequency waves have little influence on the magnetic-field distribution. [S1063-651X(99)08901-1]

PACS number(s): 52.70.Kz, 52.75.Kq

I. INTRODUCTION

Nonthermal electric fields in short-duration current-carrying plasmas strongly affect the electron collisionality and the plasma interaction with the magnetic field. We investigated the electric fields developed in a 100-ns duration coaxial plasma opening switch (POS) experiment. POS's were introduced as intermediate stages between pulse generators and loads for prepulse suppression [1], power and voltage multiplication [2], and improved coupling between generators and high impedance loads [3], on ns and μs time scales [4], at multi-TW power levels. A large effort was invested in understanding and improving the switch performance [5,6]. Plasma instabilities were suggested to affect the POS operation crucially by increasing the plasma resistivity and modifying the penetration of the magnetic field in the plasma [7]. Simulations have shown that an anomalous resistivity could enhance the magnetic-field penetration into the plasma [8,9]. It was also shown that instabilities may increase the width of the current channel in the plasma, and affect the electron heating [10–12]. It was predicted [13] that the ion-acoustic turbulence may play an important role in the POS physics. Observation of the presence of low-frequency electric fields with amplitudes up to 50 kV/cm in a microsecond duration POS, using Fabry-Perot interferometry of the H_α profile, was reported in Ref. [14] and recently in Ref. [15].

In this paper, we present observations of turbulent electric fields in a POS of 100-ns duration. The fields are determined from the time-dependent H_α and H_β spectral profiles that are spatially resolved in the radial and azimuthal directions. It is shown that during the current pulse both line profiles are dominated by the Stark effect, and are significantly broadened by nonthermal electric fields. Previous methods to study nonthermal electric fields in plasmas considered the effect of a single oscillatory field at a given frequency on the line profile [16], or assumed slowly varying quasistatic fields [17]. In this research, we apply two recently developed methods [18] to determine the amplitude and frequency of the nonthermal electric fields in the plasma. The methods make no assumptions about the field-amplitude probability distribution function or the time scale of the field fluctuations, and thus can be applied to study various instabilities over a wide range of plasma parameters.

For both methods, short and intermediate time behaviors of the level autocorrelation functions (AF's) are calculated and compared to the Fourier transforms of the observed lines. In the first method, the short-time expansion of the line AF's in the quasistatic limit, which corresponds to the wings of the line profiles, is used to determine the electric-field mean amplitude. The calculation is independent of the field frequency or the precise probability distribution function. The spectral profile measurements were extended to the line wings, giving a satisfactory accuracy in the determination of the field amplitude, as shown by the error analysis presented. In the second method, AF's of both H_α and H_β due to a single oscillatory field are calculated for various field ampli-

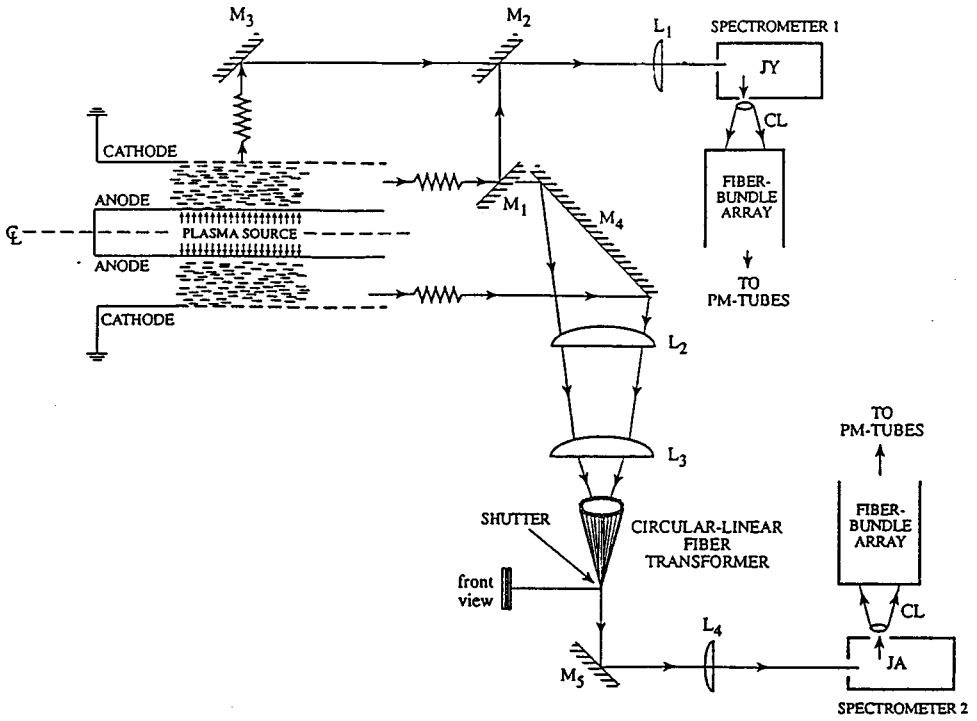

FIG. 1. Schematics of the plasma opening switch and the spectroscopic diagnostic systems. The light emitted from the plasma is collected using two optical systems into the spectrometers, enabling both axial and radial observations. The light from each spectrometer output is dispersed using a cylindrical lens (CL) on an optical fiber bundle, leading to a set of photomultiplier tubes (PMT's).

tudes and frequencies. Comparison to the experimental Fourier transforms of the two lines yields bounds on these two field parameters. The results of the two methods are in good agreement, and show the presence of instabilities in the plasma, with a typical frequency close to the plasma electron frequency and with a field amplitude of 14.5 ± 2.5 kV/cm.

The relatively high frequency of the fluctuations leads us to conclude that they result from Langmuir waves excited by fast electrons. The fast electrons can be accelerated either in a cathode sheath, or as runaway electrons if ion-acoustic anomalous resistivity occurs in the plasma. The Langmuir waves are inefficient in transferring momentum to the ions, and cannot give rise to anomalous collisionality. Therefore, the instability cannot account for the fast magnetic-field penetration into the plasma observed in the experiment [19,20], suggested to occur according to the electron-magnetohydrodynamics (EMHD) theory [10], or for the width of the current channel, observed to be much larger than the width predicted by EMHD theory. We obtain an upper limit for the amplitude of possible ion-acoustic waves, by determining an upper limit for the low-frequency electric fields, that might be obscured by the Langmuir waves. Estimates of the anomalous resistivity resulting from the ion-acoustic waves show that it is too small to affect the current distribution in the plasma and, thus, the POS operation.

II. EXPERIMENTAL SYSTEM AND DIAGNOSTICS

This study was performed using the coaxial POS described in Ref. [19], shown in Fig. 1. A positive voltage pulse (300 kV) is applied to the inner electrode by a 4 kJ, 1 Ω, water-line Marx generator, producing a 90-ns quarter-period current pulse with 135 ± 10-kA peak current. The radii of the anode and cathode are 2.5 and 5 cm, respectively. A short circuit is used as an inductive load. Typical upstream (I_u) and downstream (I_d) currents, measured by calibrated Rogowski coils, are shown in Fig. 2(a). Also shown is the current through the POS $I_{\rm pos}=I_d-I_d$. The inductive voltage drop on the plasma, calculated by $V_{\rm POS}=L_d\ (dI_d/dt)$ (L_d is the downstream inductance) reaches a peak value of 50 ± 20 kV, as shown in Fig. 2(b).

Two 1-m spectrometers, each equipped with a 2400 grooves/mm grating, giving a spectral resolution of 0.06 Å,

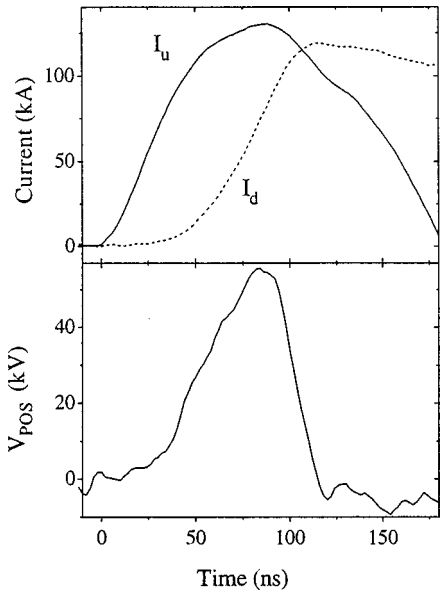

FIG. 2. The POS characteristics: (a) the upstream (I_u), downstream (I_d), and POS ($I_{\rm pos}$) currents; (b) the POS voltage $V_{\rm pos}$.

were used for the spectroscopic observations. The diagnostic system, shown in Fig. 1, allowed for axial and radial observation of the entire POS gap, using the mirrors M_1–M_4. Two imaging systems were used. One system images a rectangular section of plasma onto the spectrometer input slit using the lens L_1. The second system images an annular region of plasma using lenses L_2 and L_3 through an optical fiber bundle, that transfers a circular array viewing the plasma into a linear array, onto the spectrometer using lens L_4. Shifting the shutter at the linear array side of the optical fiber bundle allowed for different azimuths to be observed with an azimuthal resolution of $\approx 4°$. The resolution along the radial direction in the axial observation measurements is 1 mm, with similar axial resolution in the radial observation measurements. The light at each spectrometer output slit is imaged through a cylindrical lens onto an optical fiber-bundle array, and transmitted to a set of ten photomultiplier tubes, with a response time of 4 ns. The time-dependent spectral profile is recorded on a multichannel digitizer. The light dispersion, determined by the cylindrical lens system, was varied in the experiment from 0.2 Å/channel to 0.8 Å/channel, and was checked using narrow line calibration lamps. The measurements reported here are integrated over the line of sight.

A gaseous plasma gun, described in detail in Ref. [19], is installed inside the inner electrode and injects the plasma radially outward. For the investigation of the hydrogen lines, CH_4 gas was used, and the plasma is composed of protons, hydrogen and carbon up to fourth ionization stage. The plasma radial injection velocity was $(1.5\pm0.5)\times10^6$ cm/s with an axial divergence angle of $\approx 30°$. The electron temperature at the POS region, determined from C II and C III line ratios, and collisional-radiative (CR) calculations, was 2 ± 1 eV.

The plasma density prior to the current pulse was determined from hydrogen line Stark broadening, and confirmed by microwave cutoff measurements. The H_α and H_β lines were measured at several radial positions in the POS region, with the H_α and H_β FWHM's (full widths at half the maximum) being 0.75 ± 0.1 and 0.85 ± 0.15 Å, respectively. The linewidths were fitted to convolutions of Doppler (Gaussian) with Stark broadened profiles [21] to yield the electron density and hydrogen temperature, shown in Fig. 3. A quasistatic approximation was used in these Stark calculations, i.e., neglecting the effect of ion motion on the relevant time scales, which is the inverse of the line half-width at half maximum (HWHM) in the frequency domain (of the order of few ps). For the H_β line, it is well known [21] that the quasistatic approximation is adequate for our plasma parameters. For the H_α line Doppler broadening dominates the broadening and, hence, inclusion of even the most dominant Stark broadening mechanism (namely the ion dynamics [22]) affect negligibly the results.

III. MEASUREMENTS

During the current pulse the H_α and H_β lines were measured at several radial positions between $r=2.7$ and 4.8 cm (i.e., up to 0.2 cm from each electrode). Both lines were observed to broaden significantly during the current pulse, followed by a decrease at later times. A typical temporal behavior of the H_α and H_β FWHM, taken at the middle of the POS region, is given in Fig. 4, where both linewidths are seen to rise during the first 50 ns of the pulse to values higher than the initial width by $\simeq 2.5$ times. The maximum widths seen in this typical example are 1.9 ± 0.2 and 2.3 ± 0.3 Å for H_α and H_β, respectively. The H_γ line was also observed, and its width showed a similar temporal behavior. However, the H_γ low intensity did not allow for a quantitative analysis.

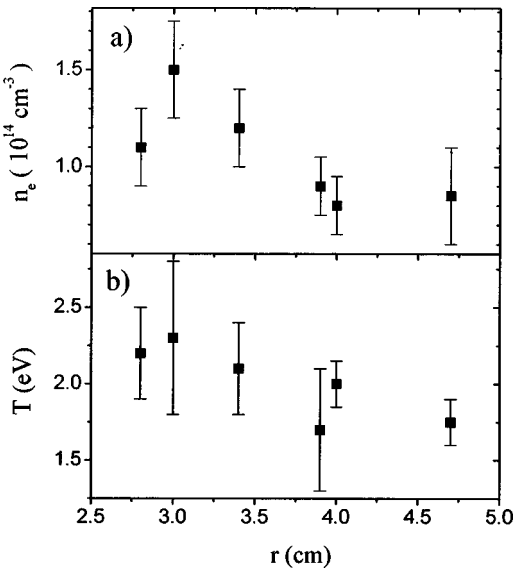

FIG. 3. The electron density (a) and hydrogen temperature (b) determined from the H_α and H_β profiles prior to the beginning of the current pulse.

The temporal behavior of the widths shown in Fig. 4 was observed at all radial and azimuthal positions, with the shot-to-shot irreproducibility at each position being $\pm15\%$. For each line, the peak widths for different positions were similar within $\pm25\%$. The temporal behavior of the two linewidths was similar at all positions within the shot-to-shot irreproducibility of ±10 ns.

Because of the relatively high accuracy of the line profiles required for the following analysis, we have verified that the hydrogen line profiles are not affected by possible nearby

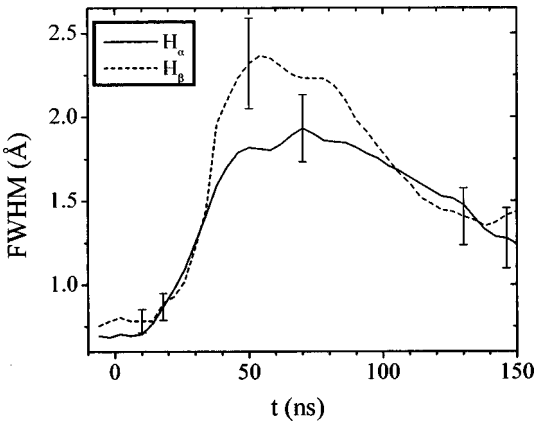

FIG. 4. Typical temporal behavior of the H_α and H_β widths (FWHM) during the current pulse at the center of the POS gap ($r=3.7$ cm). Similar behaviors are observed at all radii and azimuths.

impurity lines. To this end, we observed the intensities of various lines of species suspected to contaminate the hydrogen lines (C II, C III, N II, N III, and O II) and used collisional-radiative calculations with the electron density and temperature determined during the POS operation [19] to estimate the line intensities of these species near H_α and H_β. No impurity lines were found to be intense enough to affect the hydrogen line profiles.

In principle, an increase in the linewidths could result from an increase in the plasma density or in the hydrogen velocities. To rule out the possibility of density increase, we have performed local density measurements based on ionization times of particles with low ionization potential [19], such as Li I, Mg I, and Ba II. These measurements utilized laser evaporation of materials deposited on the inner electrode strips, to achieve axially local observations. It was shown that the plasma density did not increase from its initial value during the times of interest (up to $\simeq$80 ns after the current pulse application). Note that the observed widths cannot be explained only by an increase in the electron density, since the H_β width is affected more by thermal Stark broadening than the H_α width. In order to obtain an H_α FWHM of 2.2 Å by thermal Stark broadening at 1-eV temperature, an electron density of $n_e \approx 10^{16}$ cm^{-3} [22] is required, while a H_β FWHM of 2.2 Å results from $n_e \approx 1.2 \times 10^{15}$ cm^{-3} [23]. The electron impact contribution in our plasma parameters is only a minor correction even to the H_α Stark width (primarily determined by ion dynamical effects), hence the linewidths are insensitive to the electron temperature.

An increase in the hydrogen Doppler width, on the other hand, will have a more pronounced effect on H_α than on H_β, due to its longer wavelength. However, the hydrogen temperature cannot change appreciably during the current pulse. At our low density and short-time scale, the most efficient process in transferring momentum to the hydrogen atoms is resonant charge exchange with protons, which can gain energy during the current conduction. For energies in the range of a few tens of eV, the rate for this process is $\Gamma \leqslant 2 \times 10^{-8}$ cm^3 s^{-1} [24]. Since the proton density was estimated to be $n_p \leqslant 7 \times 10^{13}$ cm^{-3} [19], only a fraction of $\Gamma n_p t \leqslant 7\%$ of the hydrogen atoms can acquire higher velocity than their initial one during $t = 50$ ns.

Alternatively, the hydrogen velocities could increase if a substantial fraction of the hydrogen atoms would have been replaced by fast hydrogen. Fast hydrogen can be produced by charge exchange processes in the dense plasma formed near both POS electrodes [19] very early in the pulse. In order to account for the almost simultaneous width increase at all radii, the hydrogen radial velocities should have been as high as 5×10^7 cm/s. To this end, we verified, using radial observation measurements of the hydrogen Doppler shifts, that no hydrogen at such velocities is supplied during the pulse. We therefore conclude that Doppler broadening cannot significantly increase during the pulse. The effect of the magnetic field on the hydrogen line profiles was evaluated using measurements of the time-dependent magnetic-field distribution in the plasma [19,20], and was found to be small. Optical thickness effects were also estimated to be negligible. We therefore conclude that the hydrogen line broadening during the pulse is due to nonthermal electric fields. In Sec. IV we describe the determination of the amplitude and frequency of these fields.

IV. SPECTRAL LINE ANALYSIS FOR THE DETERMINATION OF THE NONTHERMAL ELECTRIC FIELDS

A. General considerations

Generally, in calculating Stark broadened line shapes, one considers the evolution of the emitter wave-functions under random electric field,

$$\mathbf{E}(t) = \mathbf{E}(t, [\alpha]), \tag{1}$$

where $[\alpha]$ is a set of random variables, solves the time-dependent Schrödinger equation for the evolution operator $U(t)$,

$$\frac{dU(t)}{dt} = -\frac{\imath}{\hbar} V(t) U(t), \tag{2}$$

and averages over the random variables.

For the thermal case, $V(t)$ is usually a dipole interaction $-\mathbf{d} \cdot \mathbf{E}(t)$, where $\mathbf{d}$ the dipole operator and $\mathbf{E}(t)$ is a time varying electric field. $\mathbf{E}(t)$ is a sum of the Debye-shielded fields produced by individual plasma particles, and $[\alpha]$ consists of particle velocities, impact parameters, times of closest approach, and angles [21,25]. Many ways were proposed for treating the dynamical effects of the plasma particles [23,26–29].

In the nonthermal case, generally neither the functional form of $\mathbf{E}(t)$ nor the parameters $[\alpha]$ and their distribution functions are known. Thus, simple models have been used, such as [16] $\mathbf{E}(t) = \mathbf{E_p} \cos(\omega_{\rm pe} t + \phi_p)$, where $\omega_{\rm pe}$ is the electron plasma frequency, or [30] $\mathbf{E}(t) = \mathrm{Re} \Sigma_k \mathbf{E}_k \exp[-i(\Omega_k + i\gamma_k)t]$, where Re denotes the real part, Ω_k is the fluctuation frequency of the field component $\mathbf{E}_k$, and γ_k is its phase. An averaging over the phase, direction, and field amplitude is performed in a perturbation-theory treatment that assumes weak interactions. Diagnoses of turbulent plasmas have utilized peculiar features of the line profiles, such as satellites [16] or dips [31]. The results of such analysis are model dependent, and may not be valid in the general case, particularly if broadband turbulence is present.

A variant of the standard thermal approach that calculates the line profile assuming that the electric field is quasistatic is also attractive for the nonthermal case [17,32–34], since it makes no assumption on the functional form $\mathbf{E}(t)$, and only requires a knowledge of the electric microfield probability distribution function (PDF) $W(E)$. However, a quasi-static treatment for some type of electric field implies a memory loss (loss of coherence) of the electron wave function that is much faster than the time scale of the field fluctuations [21]. In other words, the collisional lifetime of the level, which is the inverse of the Stark width, is shorter than the field variation time. This requirement is especially restrictive for lines such as H_α, that have a Stark component that is unaffected by quasistatic fields in the linear Stark-effect approximation, and will have a very long collisional lifetime. Therefore, a quasistatic treatment for the turbulent fields cannot be used *for the entire line profile* in low density plasmas, as in our

POS experiment, where the unshifted component broadening due to electron collisions is not large enough. Also, the quasistatic treatments usually assume a Gaussian field PDF, either isotropic (three-dimensional) or anisotropic, which occurs at a developed level of turbulence. Such a functional form may not be correct for any turbulence parameters [35].

In this study, the line shapes are analyzed by two independent methods, that we briefly presented in Ref. [18]. We make no assumptions on the origin of the fields, the exact form of their PDF, or their time scales. The only assumption is that the field length scale is significantly larger than the atomic length scale, so that the field can be regarded as spatially constant over the entire wave-function. Both methods employ the time behavior of the observed line Fourier transform, which is the experimental autocorrelation function. The AF, denoted by $C(t)$, is a linear combination of products of the evolution operators $U(t)$ of the atomic levels [36]. Using $C(t)$ in the present analysis has distinct advantages over employing the usual line profile $L(\omega)$. Since the observed widths greatly exceed the thermal widths, any thermal-nonthermal coupling can be neglected. Therefore, AF's due to different broadening mechanisms can be simply multiplied to give the total AF (see the Appendix) instead of the convolution required for analysis performed in the frequency domain. Using the time domain also enables easier identification of the different mechanisms that affect the broadening. In addition, the use of $C(t)$ is also advantages for the ''typical'' field analysis (given in Sec. IV D), since it allows for using the AF of *a single configuration (monochromatic) electric field* to evaluate the ''typical'' electric field amplitude and frequency without requiring the details of the field distribution functions (in amplitude and frequency) that are essential to construct a line profile in the frequency domain.

B. Determination of $\langle E^2\rangle$

In this section we evaluate square of the electric field $\langle E^2\rangle$, regardless of the field frequency, using the method described in Ref. [18]. The complete derivation of the formulas is given in the Appendix. The method makes use of the fact that the line wings are affected by interaction times shorter than the ones affecting the line center, and that for short enough times (far enough at the wings) any line can be treated within the quasistatic approximation. For H_α this implies that we use the parts of the profile that receive only a small contribution from the unshifted component. In the quasistatic approximation, the Stark part of the AF of a line i with a linear Stark effect can be written as the sum of the N_i Stark shifted components:

$$C^i(t)=\int dE\, W(E)\sum_{k=0}^{N_i} L_k^i\cos(ksEt), \tag{3}$$

where $W(E)$ is the field PDF, $s=1.5ea_o/\hbar$ (e is the electron charge and a_o is the Bohr radius), and $\Sigma_{k=0}^{N_i}L_k^i=1$. In the limit of short times, for pure nonthermal fields, we use in Eq. (3) the sum expressions for H_α and H_β [Eqs. (A3) and (A4) in the Appendix] and expand the cosines to obtain $C^\alpha(t)\rightarrow 1-2s^2t^2\langle E^2\rangle$ and $C^\beta(t)\rightarrow 1-\frac{62}{3}s^2t^2\langle E^2\rangle$, where $\langle E^2\rangle=\int dE\, W(E)E^2$. These values do not depend on the exact form of $W(E)$, except for the requirement that for large fields $W(E)$ decays fast enough for $\langle E^2\rangle$ to be finite (in contrast to the thermal case). This is believed to be the case for plasma turbulence, and our requirement is weaker than the Gaussian behavior frequently assumed for $W(E)$ [17,33]. Hence, if the measurements enable us to determine accurately the short-time part of the AF, they provide a *direct* measurement of $\langle E^2\rangle$.

For the case of both thermal and nonthermal fields, and a Doppler width, all having isotropic probability distribution functions, and assuming there is no correlation between them so that a convolution can be performed, we obtain the short-time behavior (see Appendix)

$$C^i(t)=1-\sum_{k=0}^{N_i} L_k^i\left[\frac{5}{2}(ksE_Ht)^{3/2}+\frac{t^2}{2}\times\left(k^2s^2\langle E^2\rangle+\frac{k_BT\omega_o^2}{Mc^2}\right)+O(t^3)\right] \tag{4}$$

where E_H is the Holtsmark field, ω_o is the unperturbed frequency of the line, T is the hydrogen temperature (or Doppler broadening), M is its mass, and c the speed of light.

In principle, for very short times, the t^2 term can be neglected and the Holtsmark field (and therefore the density) can be calculated from the limit $t\rightarrow 0$ of:

$$E_H=(1-C^i(t))^{2/3}(\tfrac{2}{5})^{2/3}(st)^{-1}\left[\sum_{k=0}^{N_i} L_k^i k^{3/2}\right]^{-2/3}. \tag{5}$$

However, the determination the Holtsmark field from the short-time behavior of $C(t)$ requires an accurate measurement of very short times, so that the Doppler and nonthermal Stark terms in Eq. (4) would be negligible. This implies an observation over a large spectral window that was not possible in our experiment because of the low light intensity at the line wings.

We also note that even in the absence of a nonthermal field, observation over a large spectral window is required in order to use Eq. (5), since the thermal field has high-frequency components (above the electron plasma frequency) and the line wings are proportional to $\omega^{-5/2}$. Since the nonthermal fields in our experiment are much stronger than the thermal fields, the AF decays faster in time and the determination of the field amplitude requires information on the line profile sections closer to its center.

In the case where the thermal field is known or can be neglected, one can divide the experimental AF by the thermal Stark AF [see Eq. (A14) in the Appendix], and obtain an equation for the nonthermal field. For small t, so that contributions from higher orders may be neglected, but not so small so that the thermal Stark contribution in Eq. (4) can be neglected, $\langle E^2\rangle$ is given by

$$\langle E^2\rangle=\left[\frac{2}{t^2}(1-\tilde{C}^i(t))-\frac{k_BT\omega_o^2}{Mc^2}\right]\left[s^2\sum_{k=0}^{N} L_k^i k^2\right]^{-1}, \tag{6}$$

where $\tilde{C}^i(t)$ is the experimental $C^i(t)$ divided by the thermal Stark AF. The value of $\langle E^2\rangle$ should be determined from times that the AF can still be treated within the quasistatic

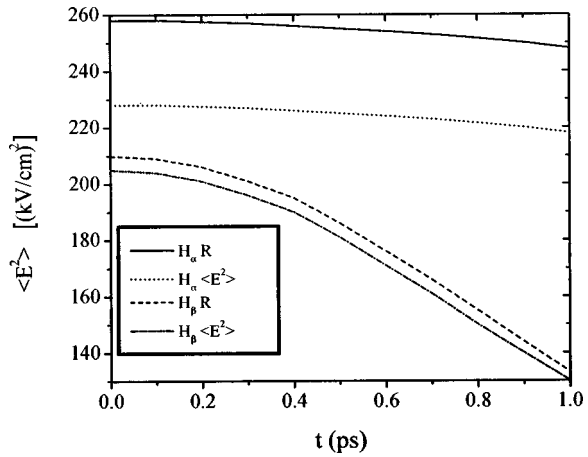

FIG. 5. Determination of $\langle E^2\rangle$ from the short-time behavior of the autocorrelation functions, $C(t)$, of H_α and H_β lines at $t=70$ ns, and $r=3.5$ cm. The solid line is R (defined in the text) calculated from the experimental $C(t)$ for H_α, and the dashed line is $\langle E^2\rangle$ obtained from R by subtraction of the Doppler contribution. The dotted and dash-dotted lines are R and $\langle E^2\rangle$ for H_β, respectively.

approximation, i.e., times considerably shorter than the field fluctuation time scale. The minimal time of the field fluctuations is the inverse of the maximal field frequency, i.e., the electron plasma frequency $\omega_{\rm pe}$, which is 1.8 ps for our experiment.

Figure 5 presents the analysis of typical H_α and H_β line profiles obtained at $r=3.5$ cm and $t=70$ ns, where the linewidths were maximal. In the figure we have plotted for each of the two lines the quantities $R\equiv[1-\tilde{C}(t)]/bs^2t^2$ and $\langle E^2\rangle = R-(1/2bs^2)(k_BT\omega_o^2/Mc^2)$ versus t, where $b\equiv\frac{1}{2}\Sigma_{k=0}^{N}L_k^ik^2=2$ for H_α, and $b=\frac{62}{3}$ for H_β. The 2-eV temperature of hydrogen and the density of 1×10^{14} cm^{-3}, determined prior to the beginning of current pulse is used in the calculations. The times used to determine $\langle E^2\rangle$ are $t\simeq0.5$ ps and $t\simeq0.2$ ps for H_α and H_β, respectively (the time required for H_β is shorter than for H_α because of its larger Stark shifts). The resulting $\langle E^2\rangle$ values are 227 kV/cm^2 for H_α (solid line) and 207 kV/cm^2 for H_β (dotted line), i.e., giving an agreement of $\approx$10%. In these times the thermal Stark $C(t)$'s drop only by 1% and 3% of the nonthermal Stark $C(t)$'s for the H_α and H_β lines, respectively, and therefore it affects the results very little.

If the temperature is not known, H_α and H_β can be treated self-consistently to yield both $\langle E^2\rangle$ and T. For the example given in Fig. 5, such a procedure gives $\langle E^2\rangle=200$ kV/cm^2 and $T=3.7$ eV. It is seen that the difference between the values $\langle E^2\rangle$ determined by the self-consistent analysis and the values obtained in Fig. 5 are small, and within the error bars discussed in Sec. IV C. The hydrogen temperature inferred has a large relative error (with respect to the 2.0 $\pm$0.3-eV value), which evidently results from the fact that the Doppler contribution to the line profile in this example is much smaller than that of the nonthermal fields.

C. Error analysis

In order to verify whether the accuracy in the determination of the experimental AF is sufficient to allow for a reliable determination of $\langle E^2\rangle$, an error analysis was performed. Let $L(\omega)$ denote the experimentally measured profile, and let the true profile be $L(\omega)+\delta L(\omega)$. Let $C_e(t)$ and $C_t(t)$ denote the experimental and ''true'' AF's, respectively, i.e.,

$$C_e(t)=\frac{\int e^{i\omega t}L(\omega)d\omega}{\int L(\omega)d\omega},$$

$$C_t(t)=\frac{\int e^{i\omega t}[L(\omega)+\delta L(\omega)]d\omega}{\int [L(\omega)+\delta L(\omega)]d\omega}. \tag{7}$$

The relative error $\Delta C(t)$ in the quantity $1-C_e(t)$, from which $\langle E^2\rangle$ and T are determined [and are linear in $1-C_e(t)$], is $\Delta C(t)=[C_t(t)-C_e(t)]/[1-C_t(t)]$. The relative error may be expressed as

$$\Delta C(t)=\frac{r_0[r_1(t)-C_e(t)]}{1-C_e(t)+r_0[1-r_1(t)]}, \tag{8}$$

where

$$r_1(t)=\frac{\int e^{i\omega t}\delta L(\omega)d\omega}{\int \delta L(\omega)d\omega} \tag{9}$$

and

$$r_0=\frac{\int \delta L(\omega)d\omega}{\int L(\omega)d\omega}. \tag{10}$$

Here r_0 is a measure of the accuracy of the experiment, an integrated error-to-signal ratio, where r_1, the Fourier transform of the error, represents the error spectrum.

For short times, $C_e(t)$ is a number close to unity, and so is r_1, while r_0 is usually a small number. Hence, in the final expression for ΔC [Eq. (8)], the numerator is the product of two small numbers, while the denominator is a sum of two small numbers. However, r_0, which could in principle be negative, is usually a higher order correction. In practice, in order to obtain a small relative error one needs $r_0[1-r_1(t)]\ll 1-C_e(t)$.

There are two main sources of error in the experiment. The first comes from the limited spectral window observed, which imposes a cutoff at a certain frequency, and thus produces a missing frequency range (MFR) in the Fourier transform. The second source is uncertainties in the experimental spectrum due to noise, in our case electrical (rf) and shot noise. Other sources of errors, including the numerical procedure to obtain the AF from the line profile that is based on a Filon integration, do not introduce significant additional errors.

In our experiment, the maximal spectral window observed in a single shot was up to 4 Å from the line center for H_α and up to 6 Å for H_β. The maximal MFR error in a single shot

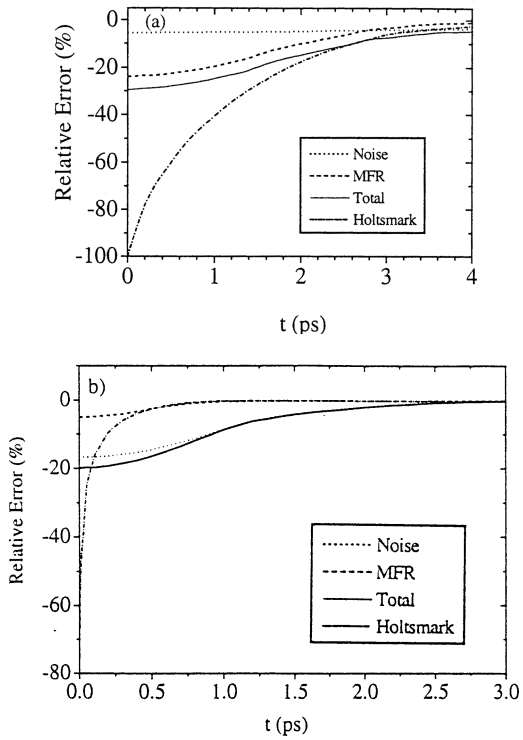

FIG. 6. The relative error in $1-C(t)$ determined from the short-time behavior of the AF's for (a) H_α and (b) H_β. The dot-dashed lines are the MFR errors assuming a Holtsmark tail for frequencies above the single-shot spectral window, and the dashed lines are the MFR with the empirical extrapolation formula given in the text. The dotted lines are the error due to the positive noise amplitude (using the top of the data points error bars), and the solid lines are the sum of the noise and extrapolated MFR errors.

can be evaluated by assuming that we have measured the line profile up to a frequency ϖ. In this case $L(\omega)=L(\omega)\theta(\varpi-|\omega|)$ and $\delta L(\omega)=\delta L(\omega)\theta(|\omega|-\varpi)$, where $\theta(|\omega|-\varpi)$ is the Heaviside function. Since the largest relative error occurs when the wings have the slowest decrease with frequency, let us first assume that the profile outside the observation window decreases as in the thermal (Holtsmark) case, i.e., $\delta L(\omega)=A|\omega|^{-5/2}$ for $|\omega|\leqslant\varpi$. From continuity, $A=\varpi^{5/2}L(\varpi)$.

Assuming an Holtsmark behavior of the wings gives a maximum value for r_0: $r_0=(2|\varpi|[L(\varpi)+L(-\varpi)])/[3\int_{-\varpi}^{\varpi}L(\omega)d\omega]$ and gives the relative errors shown by the dash-dotted lines in Figs. 6(a) and 6(b). For the typical time used in Sec. IV B for the determination of $\langle E^2\rangle$ from H_α, the relative error in a single shot can be as large as 60% at $t=0.5$ ps [Fig. 6(a)]. For H_β, we obtain a relative error of 9% at $t=0.2$ ps [Fig. 6(b)].

By the definition of $L(\omega)$ and $\delta L(\omega)$ the error in the line profile $\delta L(\omega)$ due to the MFR is always positive, making r_0 positive. Since C_e drops more slowly than $r_1(t)$, for short enough times, $r_0[1-r_1(t)]$ could be the dominant term in the denominator of ΔC [Eq. (8)]. As a result the relative error can reach 100% at $t=0$ [$r_1(t)<C_E$ in the numerator of Eq. (8)]. This is expected since the lack of data at frequencies above ϖ preclude obtaining information at $t=0$. However, as both C_e and $r_1(t)$ decrease at longer times, the r_0 factor (which is <1) makes the $1-C_e(t)$ term the dominant one in the denominator. The relative error is then

$$\Delta C=\frac{r_0[r_1(t)-C_e(t)]}{1-C_e(t)}. \tag{11}$$

The key question is whether $1-C_e(t)$ drops fast enough to become the dominant term in the denominator at times that preserve the validity of the quasistatic assumption and the short-time expansion of the AF. This clearly depends on the quality of the experimental profile, namely, r_0, and the following error analysis shows that satisfactory accuracy can also be obtained for H_α if measurement of shorter times is performed.

In order to reconstruct the line wings away from the line center, we have performed measurements with the spectral window shifted from the line center. The experimental line profiles were fitted with an empirical function of the form $L(\lambda)=A[1+c\lambda^{5/2}]^{-1}\exp(-a[a\lambda/(1+b\lambda)])$, that has the asymptotic behavior of the Holtsmark field PDF at large wavelength shifts from the line center. This empirical profile drops faster than in the Holtsmark case assumed above, and, therefore, gives a much smaller relative error. With these profiles as the MFR $\delta L(\omega)$, the error resulting from the MFR does not exceed 25%, as shown by the dashed lines in Figs. 6(a) and 6(b).

As stated above, the second source of error is noise. Near the line center the number of photons is large, the noise is dominated by shot noise, and the signal-to-noise ratio is relatively large. Toward the wings, the photon number decreases, and the noise becomes dominated by the electrical noise. Thus the observation of the far line wings, in order to reduce the MFR error, is limited by the electrical noise.

To estimate the error due to noise in the experiment, we have evaluated the maximum noise amplitude, based on the electrical and shot noise for each section of the line profile. We then defined a noise level function that depends on wavelength that decreases with wavelength displacement from the line center until it becomes constant. Calculations of the error according to Eq. (12) were performed using this noise level function for $\delta L_N(\omega)$ added to the data points. This calculation, that uses the tops of the error bars of each of the data points, gives a line profile broader than $L(\omega)$. The results of this procedure are shown by the dotted lines in Figs. 6(a) and 6(b). The solid lines in these figures are the total error (noise plus MFR), calculated using the additivity of r_1 and r_0:

$$r_1(t)=\frac{\int \delta L_{\mathrm{MFR}}(\omega)e^{i\omega t}d\omega+\int \delta L_N(\omega)e^{i\omega t}d\omega}{r_0\int L(\omega)d\omega}. \tag{12}$$

The total relative errors in the determination of $1-C(t)$ are smaller than 25% for both H_α and H_β.

Since the noise is also negative, we have performed similar calculations with a negative $\delta L_N(\omega)$ in Eq. (12), with the same noise amplitude, i.e., using the bottoms of the error bar of each of the data points. The results for H_α and H_β are shown in Figs. 7(a) and 7(b), respectively. The noise error (dotted lines) is now positive and cancels part of the MFR error (dashed lines), resulting in a total relative error $\leqslant 20\%$.

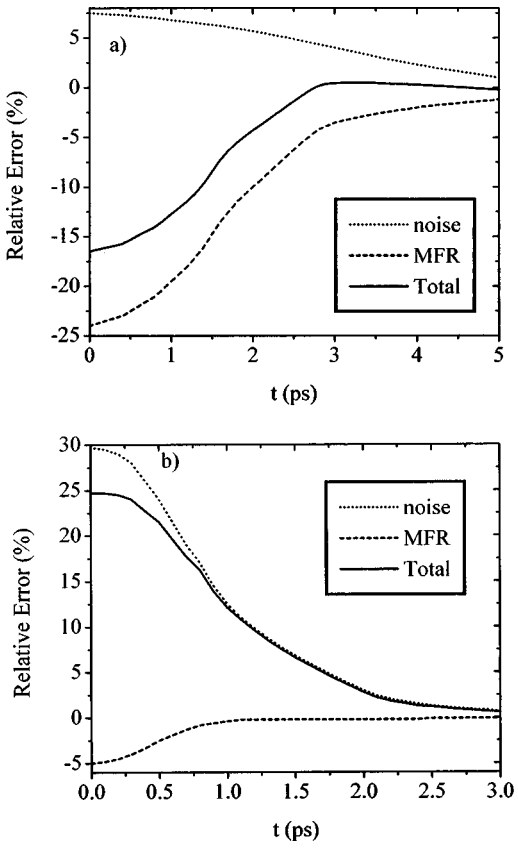

FIG. 7. The relative error in $1-C(t)$ with negative noise amplitude (using the bottom of the data points error bars) for (a) H_α and (b) H_β. The dashed lines are the extrapolated MFR error, the dotted lines are the error due to the noise, and the solid lines are their sums.

We note that these relative errors are in fact an upper limit since our treatment considered the maximum noise amplitude.

D. Typical-field analysis

In order to obtain an estimate of the electric-field fluctuation frequency and to examine further the results given in Sec. IV B, we performed calculations of the AF's for H_α and H_β by solving the Schrödinger equation for the contribution of an oscillatory field with a given amplitude and frequency. Such a monochromatic field represents a single realization of the stochastic microfield distribution in the plasma. Let $\overline{C}(t)$ denote the contribution of this oscillatory field to the AF, $C(t)$ [$C(t)$ is obtained by averaging over many $\overline{C}(t)$'s due to different realizations of the stochastic field $E(t)$ [36]]. Each $\overline{C}(t)$ is unity at $t=0$, decreases for short and intermediate times, and oscillates for long times. For long times, contributions from different realizations have random phases and the averaged AF decays to zero. Here we compare the experimental AF to calculated $\overline{C}(t)$'s for short and intermediate times (thus avoiding the averaging required to reconstruct a line profile) in order to obtain bounds on the typical field amplitude and frequency. Although such a comparison neglects the distribution functions of the electric fields, it gives bounds for the typical nonthermal field amplitude and frequency. However, such a single realization cannot be used to construct a line profile, since $\overline{C}(t)$ of a single realization does not decay to zero at long times and its Fourier transform will almost be a δ function. Hence the analysis performed in this section cannot be done in terms of line profiles, since the linewidth is not simply the inverse of the decay rate of $\overline{C}(t)$.

In what follows, we will refer to the ''amplitude'' and ''frequency'' of the typical oscillatory field, although in the plasma both are stochastic quantities. This is to be understood in an average sense, since the mean values of the true field amplitude or frequency should be similar to those of that typical field that is found to give an AF similar to the experimental one. A more accurate determination of the field parameters based on averaging over stochastic $\overline{C}(t)$'s requires further assumptions on the distribution functions of the field amplitude and frequency. Such an analysis was not performed in the present paper.

A lower bound on the fluctuation frequency of the field can be readily obtained by noting that H_α, having a strong unshifted component, is much less sensitive to quasistatic fields than H_β. A quasistatic nonthermal field will result in a much larger width for H_β than H_α, in contradiction to the experimental results. Hence, for explaining the fast decay of the H_α AF (i.e., the H_α large width), a nonquasistatic field is essential. Since the thermal-field effects on H_α are negligible in our case, the turbulent field can be considered quasistatic if its frequency is much lower than the experimental HWHM of the line [21], which in our experiment is about 3×10^{11} Hz. Therefore, fields with a fluctuation frequency less than $\Omega\approx3\times10^{10}$ Hz can be considered quasistatic, and thus the field fluctuation frequency Ω in our experiment must exceed this value [we have verified that for $\Omega=3\times10^{10}$ Hz, $\overline{C}(t)$ is practically identical to that obtained for zero frequency for the field amplitudes considered]. The upper limit for the frequency of the instability is the electron plasma frequency, thus Ω has to be in the range 3×10^{10} Hz$\leqslant\Omega\leqslant6\times10^{11}$ Hz.

For an electric field that cannot be assumed to be quasistatic, the field fluctuation frequency has an important effect on the decay rate of $\overline{C}(t)$. For the same field amplitude, the higher is the fluctuation frequency the slower the decay of $\overline{C}(t)$. This can be seen from the Schrödinger equation for the evolution operator [Eq. (2)] that determines $\overline{C}(t)$. Suppose that a field of a certain amplitude and a frequency Ω_0 that is close to the quasistatic limit causes $U(t)$ (that is unity at $t=0$) to drop appreciably at a time $\tau\simeq\Omega_0^{-1}$. A field of the same amplitude, but with a higher frequency $\Omega>\tau^{-1}$, will cause $U(t)$ to drop a little during the short time Ω^{-1}. After this time, $V(t)=-\mathbf{d}\cdot\mathbf{E}(t)$ changes sign and $U(t)$ starts increasing. This results in oscillations close to unity, and therefore in a slower net decay of $\overline{C}(t)$. For a given field frequency, a stronger field would result in a faster decay of the $\overline{C}(t)$. The above considerations would also apply to thermal broadening. However, in the thermal case the field amplitude and the fluctuation frequency are not independent.

The dependence of the H_β profile on the turbulent field amplitude and frequency is different from that of H_α because of the absence of the unshifted component for H_β. Therefore, employing this typical field analysis to both lines allows for a determination of both the typical amplitude and frequency. However, for our frequency range and for the H_β

widths observed, the H_β profiles are rather insensitive to the field frequency. This allows the field amplitude to be determined from the H_β profile with little dependence on the frequency.

In order to estimate the typical field parameters in our experiment, we have calculated $\overline{C}(t)$ with a field of the form $\mathbf{E}(t)=(E_0/\sqrt{2})\times[\cos(\Omega t)\hat{\mathbf{x}}+\sin(\Omega t)\hat{\mathbf{y}}+\cos(\Omega t+\phi)\hat{\mathbf{z}}]$ for various Ω's in the range determined above. The phase ϕ was added to make the electric field three dimensional. The choice of the phase is rather arbitrary, and as long as it is not close to 0 or $\pi/2$ the results are insensitive to its exact value for short and intermediate times (in the calculations presented here, $\phi=0.2$). E_0, the value of $\mathbf{E}(t)$ at $t=0$, is expected to be similar to value of $\sqrt{\mathbf{E}^2}$ determined in Sec. IV B. With this electric field as a perturbation, the Schrödinger equation was integrated numerically, using the method of Ref. [37].

Figure 8 shows the results of calculations of $\overline{C}(t)$ for H_β, and the experimental AF used for the calculation given in Sec. IV B. In each figure the solid lines are the experimental nonthermal $\tilde{C}(t)$ (defined in Sec. IV B), obtained by dividing the experimental $C(t)$ by the thermal one. In the calculations, the plasma density was assumed to be 1×10^{14} cm^{-3} and the hydrogen temperature 2 eV. Also shown are $\overline{C}(t)$'s calculated for field amplitudes of $E_0=7$ kV/cm (dashed lines), 14.5 kV/cm (dotted lines), and 20 kV/cm (dash-dotted lines), for four field fluctuation frequencies: 3×10^{10} Hz [Fig. 8(a)], 1×10^{11} Hz [Fig. 8(b)], 3×10^{11} Hz [Fig. 8(c)], and 6×10^{11} Hz [Fig. 8(d)], the highest frequency being ω_{pe}. It can be seen that for the frequencies considered here, $\overline{C}(t)$ for H_β is rather insensitive to the fluctuation frequency of the field at short and intermediate times, i.e., until $\tilde{C}(t)$ dropped considerably from unity, at a time about 2 ps. For $t\lesssim1$ ps the $\overline{C}(t)$'s for a field amplitude of $\approx$14.5 kV/cm match the experimental $\tilde{C}(t)$ at all the frequencies considered. This result is in good agreement with the result obtained in Sec. IV B, where the field amplitude was determined to be $\sqrt{\langle E^2\rangle}=14.5\pm2.5$ kV/cm, although the times used here are significantly larger (in Sec. IV B, times of $\lesssim0.2$ ps were used for H_β). For longer times, the experimental AF decays more slowly and fits the calculations with fields of smaller amplitude between 8 and 11 kV/cm for frequencies of 3×10^{10} and 6×10^{11} Hz, respectively.

Figure 9 shows the experimental nonthermal $\tilde{C}(t)$ and the calculated $\overline{C}(t)$'s for H_α at the same field parameters used for H_β. It can be seen that at short times (for H_α the short times are $t\lesssim2.5$ ps) the $\overline{C}(t)$'s of fields with amplitude of 14.5 kV/cm, for all frequencies, are closer to the experimental AF. At short times, the field with amplitude $E_0=20$ kV/cm cause $\overline{C}(t)$ to decay faster than $\tilde{C}(t)$, while the field of $E_0=7$ kV/cm results in too slow a decay. This result is expected since, based on the observed H_α width, for all the frequencies considered here these short times are close to the quasistatic limit, which was used in Sec. IV B, and yielded $\sqrt{\langle E^2\rangle}=14.5\pm2.5$ kV/cm.

We will now use the intermediate times for H_α ($4\text{ ps}\leqslant t\leqslant8$ ps) to obtain an estimate of the typical field fluctuation frequency. At the low frequencies [3×10^{10} and 1×10^{11} Hz;

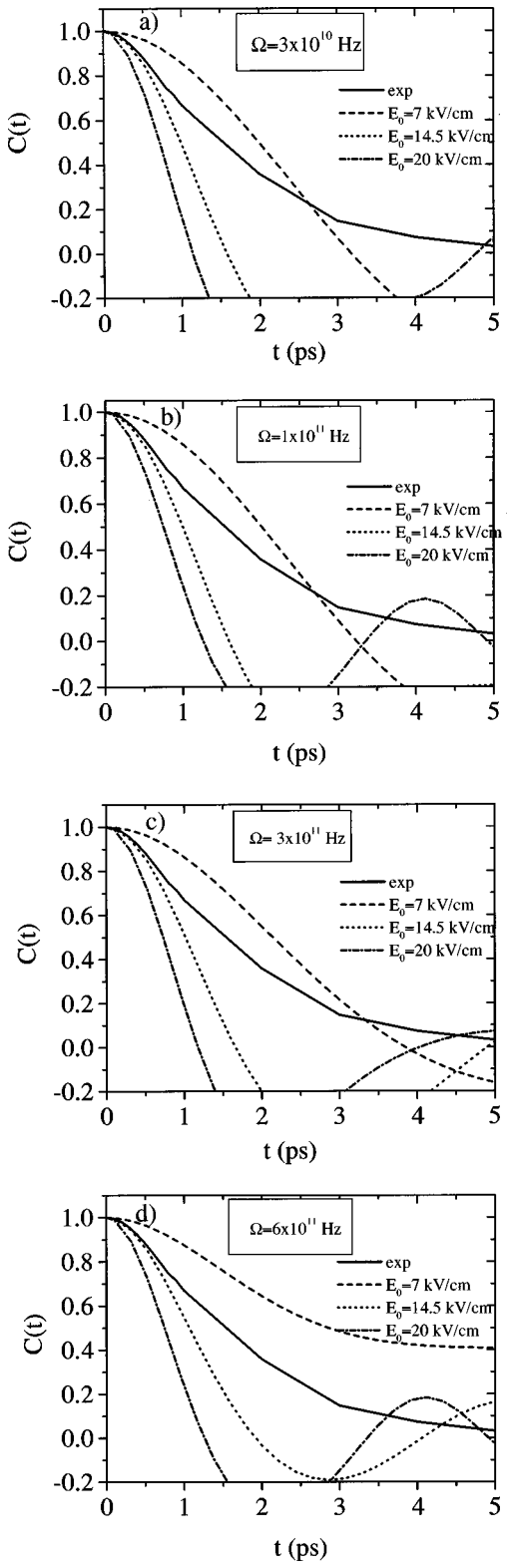

FIG. 8. The experimental nonthermal AF (i.e., the experimental AF divided by the thermal Stark and Doppler contributions) of H_β, given by the solid lines, and calculated AF's for several amplitudes and frequencies of the oscillatory electric field. The oscillatory field amplitudes are 7 kV/cm (dashed lines), 14.5 kV/cm (dotted lines), and 20 kV/cm (dash-dotted lines). The fluctuation frequencies are (a) 3×10^{10} Hz, (b) 1×10^{11} Hz, (c) 3×10^{11} Hz, and (d) 6×10^{11} Hz.

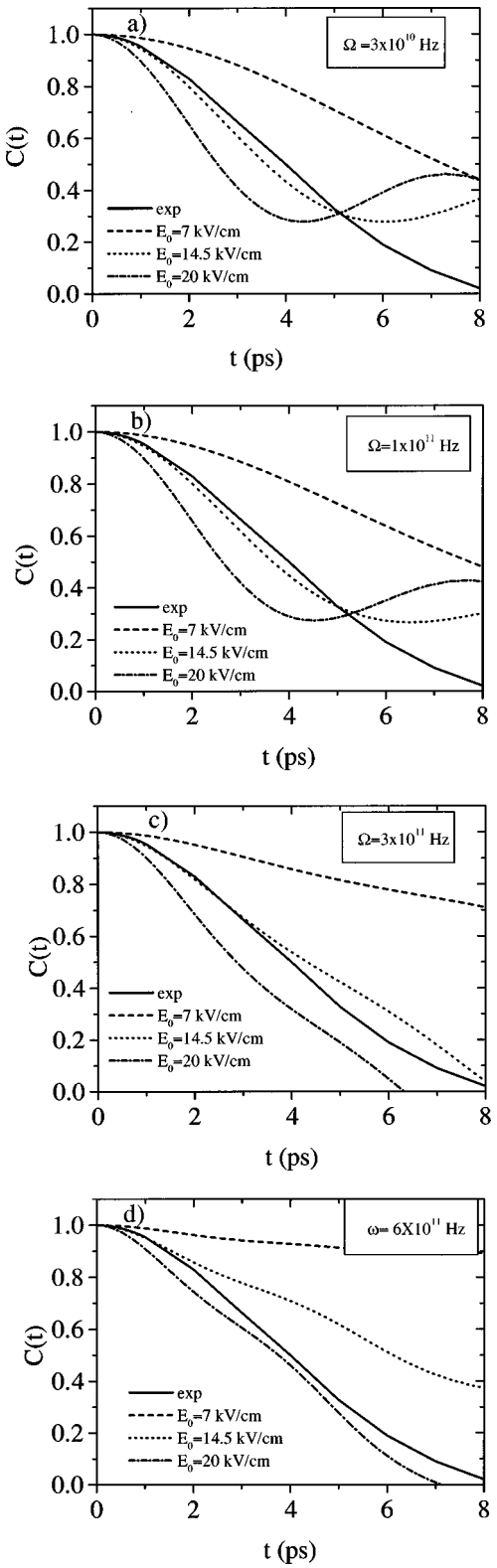

FIG. 9. The experimental nonthermal AF (i.e., the experimental AF divided by the thermal Stark and Doppler contributions) of H_α, given by the solid lines, and calculated AF's for several amplitudes and frequencies of the oscillatory electric field. The oscillatory field amplitudes are 7 kV/cm (dashed lines), 14.5 kV/cm (dotted lines), and 20 kV/cm (dash-dotted lines). The fluctuation frequencies are (a) 3×10^{10} Hz, (b) 1×10^{11} Hz, (c) 3×10^{11} Hz, and (d) 6×10^{11} Hz.

Figs. 9(a) and 9(b), respectively] the $\bar{C}(t)$'s for $E_0=14.5$ kV/cm increase at the intermediate times and decay more slowly than the experimental $\tilde{C}(t)$. The $C(t)$'s obtained by averaging over various frequencies in this low-frequency range (but over fields with the same amplitude) will not decay as fast as $\bar{C}(t)$, since all $\bar{C}(t)$'s at these frequencies have almost the same phase, and decay more slowly than $\bar{C}(t)$. Averaging over various field amplitudes at a given frequency in this low-frequency range will also not produce a decay as fast as the experimental one at the intermediate times. As can be seen from Figs. 9(a) and 9(b), even the $\bar{C}(t)$'s produced by a field amplitude of 20 kV/cm [which is much too high, as can be seen from the calculations for H_β (Fig. 8) and from the results given in Sec. IV B] decay more slowly than $\tilde{C}(t)$.

In order for the $\bar{C}(t)$'s of H_α produced by a field with an amplitude $E_0=14.5$ kV/cm to decay similar to the experimental $\tilde{C}(t)$ for both short *and* intermediate times, a frequency as high as $\Omega=3\times10^{11}$ Hz is required. For $\Omega=6\times10^{11}$ Hz, a field with an amplitude of $\approx$18 kV/cm (again, quite close to the results obtained in Sec. IV B) is needed to match the experimental AF. To conclude, this analysis shows that the typical electric field in the plasma has an amplitude of 8–18 kV/cm (obtained from H_α and H_β), and a fluctuation frequency of $(3-6)\times10^{11}$ (obtained from H_α). The field amplitude obtained here is in good agreement with that obtained in Sec. IV B.

We have also examined the possibility of the presence of both low- ($\Omega<10^{11}$ Hz) and high-frequency ($\Omega>3\times10^{11}$ Hz) fields in the plasma. If both fields are stochastically independent, the net AF decay would be given by the product of the individual AF's (this is in fact true under more general circumstances [38]). The low-frequency field has little effect on the H_α profile, as discussed above, and, therefore, a high-frequency field of at least 13 kV/cm is required in order for the calculated $C(t)$ to match the experimental one. Adding low-frequency fields of various amplitudes to this high-frequency field and comparing the H_β, $C(t)$'s show that the low-frequency field cannot exceed 5 kV/cm. This value is also in agreement with the difference between the maximal and minimal values of the electric field determined in Sec. IV B.

We note that, in principle, it is possible that fields much different from the typical field exist in the plasma. However, as shown here, most of the field distribution should be close to the typical parameters determined here, in order for the calculated AF's to fit the experimental ones.

V. DISCUSSION

The high-frequency nonthermal (turbulent) electric fields observed in the POS plasma have a typical frequency close to ω_{pe} and above the electron cyclotron frequency (Ω_{ce}), that is $\leqslant 10^{11}$ Hz in our experiment. The fields cannot result from current-driven magnetized modes since the magnetic field in our plasma is not strong enough for such modes to grow. The reason for this is that they are stabilized by the quasilinear effects, even though the current flow velocity exceeds the threshold for their excitation [39,40]. The condition for the magnetized modes to become significant is $\Omega_{ce}>\omega_{pe}$, which for our experiment, $n_e\simeq1\times10^{14}$ cm^{-3}, re-

quires $B>3\times10^4$ G, while the maximum value of the magnetic field is 10^4 G.

A plausible explanation of the high-frequency fluctuations is the presence of Langmuir potential waves, which are fully electron modes in the sense that they do not interact with the ions. Therefore, any scenario of the Langmuir waves (except for nonlinear mechanisms) includes fast electrons as a source for their excitation [40,41]. The beam-plasma interaction that causes the resonant excitation of the Langmuir waves should fulfill the Cherenkov resonance condition

$$\omega=\mathbf{k}\cdot\mathbf{V}, \tag{13}$$

where ω is the wave frequency, $\mathbf{k}$ is the wave vector, and $\mathbf{V}$ is the electron velocity. This condition can be readily satisfied in the case of fast electrons with a velocity V_f that considerably exceeds the thermal velocity V_{Te}.

The basic scenario for the generation of such fast electrons is the formation of a voltage drop as a result of a current-driven instability. This potential drop accelerates some fraction of the plasma electrons which, in turn, excite the plasma waves observed in our experiment. In principle, current-driven instability may result in both the formation of an electrostatic sheath and/or turbulent (anomalous) resistivity. A sheath may be formed near the cathode as a result of the current-driven Buneman instability in its nonlinear stage, that follows the pure EMHD (conduction) phase [42,43]. The condition for the excitation of this hydrodynamical two-stream instability is that the current flow velocity is higher than the electron thermal velocity, i.e., $j>n_e eV_{Te}$, which probably occurs in our experiment. There are experimental [44,19] and theoretical [45,46] arguments that such a sheath is indeed formed in the POS. Although such a sheath, that follows EMHD dynamics, is not expected to cover the entire cathode surface at any instant, and although the electron flow across the sheath may be suppressed due to magnetization [43,47], the leakage of electrons accelerated through the sheath may be sufficient to provide the observed level of Langmuir oscillations [48]. Unlike ion-acoustic waves, the damping rate of the Langmuir waves (see, e.g., Refs. [39,40]) is rather small if $kr_D<1$, where r_D is the Debye radius (this condition is just equivalent to $V_f>V_{Te}$). As a result, the free path length of Langmuir quanta (plasmons) is high enough to provide the filling of the whole POS gap by the high-frequency waves [48], despite a wave generation that is localized in space. Let us note that any sheath located close to the anode (that does appear within the frame of some theoretical models [11,46]) will not cause the injection of fast electrons in the plasma.

Another possibility to produce the fast electrons is a voltage drop due to an anomalous resistivity [48,49]. It is important to note that, since $\Omega_{ce}<\omega_{pe}$, ion-acoustic waves appear to be the only mechanism for giving rise to both anomalous resistivity and plasma turbulent heating (magnetized modes are not efficient in producing these two effects). The ion-acoustic turbulent scenario results from the fact that in this case the effective collisional frequency depends on the particle velocity similar to the Lorentz plasmas: $\nu_{\rm eff}\propto v^{-3}$ [48,50]. The turbulent resistivity forms a voltage drop in which the plasma electrons are accelerated. Since the effective collisions cannot provide an efficient friction to slow down the faster electrons, runaway of electrons occurs. In fact, within the frame of the quasilinear theory, non-Maxwellian particle distributions may be formed [41,48]. Although in a regime of anomalous resistivity the fraction of the runaway electrons out of the total number of electrons is small, and the beam current is small compared to the net current, the runaway electrons can efficiently excite the Langmuir waves.

We now examine the possible effects of the turbulence on the magnetic-field and current distributions in the POS. We first note that the temporal behavior of the linewidths, shown in Fig. 4, resembles the time dependence of the current conducted through the POS [$I_{\rm pos}$ in Fig. 2(a)]. It was shown in Sec. III that the lines are broadened by the turbulent electric fields. Although the measurements are integrated along the axial line of sight, the increase in the widths result from the increase in time of the field amplitude and not from the spatial widening of the turbulent region. This is concluded from the fact that the electron temperature increases significantly in the regions where the current is conducted, and the light emitted from these regions dominates the hydrogen line profiles. The increase in the field amplitude during the pulse probably results from the increase of the energy of the electrons which excite the waves. In what follow we would use the peak electric field determined in Sec. IV in order to obtain an upper bound on its influence on the magnetic-field distribution.

The time-dependent, three-dimensionally resolved, magnetic-field distribution in our experiment was measured from Zeeman splitting [20], and inferred from ion velocities [19]. The results show that the magnetic field penetrates the plasma at a velocity of $\approx10^8$ cm/s, which is almost three orders of magnitude higher than the collisional diffusion velocity. The magnetic-field evolution was explained by an analytical EMHD model [20]. It was also found that at $t\gtrsim40$ ns most of the current flows in a channel of width $\gtrsim2$ cm (significantly larger than the experimental spatial resolution that is $\lesssim1$ cm). The observed width is two orders of magnitude larger than the classical skin depth, based on the Spitzer resistivity, which is the width expected from the EMHD model. The Langmuir waves found here cannot contribute to anomalous resistivity since they cannot satisfy the Cherenkov resonance condition with ions. To transfer momentum to ions efficiently, the typical phase velocity has to be comparable to the ion velocity, i.e., $\omega/k\leqslant V_{Ti}$ in accordance with Eq. (13), which is not fulfilled for Langmuir waves for which $\omega/k>V_{Te}$. Therefore, the Langmuir waves cannot be responsible for either the fast field penetration or for the broad current channel observed in our experiment.

Let us estimate the magnetic-field penetration velocity and the width of the current channel if some level of the low-frequency (ion-acoustic) waves had been excited in the plasma. Although the H_α and H_β Stark broadening is dominated by high-frequency oscillations, some level of low-frequency electric fields, which is lower than that caused by the Langmuir waves, can be present. The effective collisional frequency $\nu_{\rm ei\,eff}$, resulting from the ion-acoustic turbulence, may be roughly approximated by [51,52]

$$\nu_{\rm ei\,eff}\simeq\omega_{\rm pe}\frac{\langle E^2\rangle}{8\pi n_e T_e}. \tag{14}$$

The diffusion frequency υ_D of the magnetic-field penetration can be estimated using:

$$\nu_D=\frac{n_e e^2}{m}\eta=\frac{n_e e^2}{m}\frac{4\pi L^2}{c^2\tau_D}=\left(\frac{\omega_{\rm pe}L}{c}\right)^2\frac{1}{\tau_D}, \qquad (15)$$

where L is the plasma length and τ_D is the diffusion time. Using Eqs. (14) and (15), the diffusion time can be expressed as

$$\tau_D=\left(\frac{\omega_{\rm pe}L}{c}\right)^2\frac{8\pi n_e T_e}{\omega_{\rm pe}\langle E^2\rangle}. \qquad (16)$$

In our experiment, $n_e=10^{14}$ cm^{-3}, $L=4$ cm, and $T_e=10$ eV (determined as a lower limit for the electron energy during the POS operation [19]). An electric field $E=5$ kV/cm, determined in Sec. IV D as the upper limit for the low-frequency field, gives an anomalous collision frequency of $\nu_{\rm ei\ eff}=4\times10^9$, and a diffusion time of $\simeq1.5$ μs. With the same parameters we find that an ion-acoustic turbulence producing an electric field of $\simeq30$ kV/cm is required in order to explain the magnetic-field penetration observed in the experiment.

The width of the current channel, δ_B, calculated by the EMHD theory [51], is given by

$$\delta_B\simeq\frac{c^2}{4\pi\sigma}\frac{a\omega_{\rm pi}/c}{V_A}\simeq a\frac{\nu_{\rm ei\ eff}}{\omega_{\rm pe}}\frac{c}{V_{Ae}}, \qquad (17)$$

where a is the typical space scale in the direction normal to the electrodes and σ is the plasma conductivity. This width can also be expressed as $\delta_B\sim a(\nu_{\rm ei\ eff}/\omega_{Be})$. Inserting Eq. (14) into Eq. (17), we obtain the width of the current channel:

$$\delta_B\simeq a\frac{c}{V_{Ae}}\frac{\langle E^2\rangle^{LF}}{8\pi n_e T_e}=a\frac{\omega_{\rm pe}}{\omega_{Be}}\frac{\langle E^2\rangle^{LF}}{8\pi n_e T_e}. \qquad (18)$$

Taking $E=5$ kV/cm, $T_e=10$ eV, and a typical scale $a=2$ cm, we obtain that the width of the current channel is $\delta\leqslant0.1$ cm. Therefore, these estimates suggest that the width of the current channel observed in our experiment does not result from anomalous resistivity.

It is interesting to compare the upper limit here obtained for the amplitude of the electric field produced by ion-acoustic waves in the plasma, to those predicted in theoretical treatments for the POS problem. In Ref. [7], it was suggested that the electric field is expected to saturate at an amplitude $E=T_e\lambda_D^{-1}$, where T_e is the electron temperature (in eV) and λ_D is the Debye length. For $T_e=10$ eV, one obtains amplitude of 43 kV/cm. The treatment of Sudan and Similon [53] takes into account quasilinear effects and predicts that the electric-field saturation amplitude would be $E=T_e\lambda_D^{-1}(W\Omega_e\lambda_D/\upsilon_{\rm te}^2)^{1/3}=T_e\lambda_D^{-1}(W/\upsilon_{\rm te}\Omega_e/\omega_{\rm pe})^{1/3}$ (here W is the electron drift velocity, $\upsilon_{\rm te}$ is the electron thermal velocity, Ω_e is the electron cyclotron frequency, and $\omega_{\rm pe}$ is the plasma frequency). This treatment gives a smaller amplitude $E=21$ kV/cm for $T_e=10$ eV. The latter calculation of the field amplitude requires an assumption on the electron drift velocity. For this estimate we have assumed the minimum velocity possible for our experiment (i.e., we assumed that the current flows across the entire plasma) in order to obtain a lower limit for the predicted field amplitudes. It is seen that the upper limit inferred for our data (5 kV/cm) is significantly lower than the lower limits predicted by these theoretical treatments. This also strengthens the conclusion that the ion-acoustic turbulence does not play a significant role in our POS.

VI. SUMMARY

Two methods, introduced in Ref. [18], were applied to investigate the amplitude and frequency of nonthermal electric fields in a high-current carrying plasma using the spectral line shapes of the Stark broadened H_α and H_β. The methods use short- and intermediate-time behaviors of the Fourier transforms of the measured line profiles to obtain the amplitude and frequency of the electric fields. One method uses the short-time (quasistatic) behavior of the autocorrelation function to determine the electric-field amplitude independently of its frequency. In principle, this method can also be used to determine the contributions of the Doppler effect and of the particle electric fields to the line profiles (see the Appendix). However, in our experiment these contributions were determined from independent measurements [19]. After subtracting them from the experimental line profiles, the two hydrogen lines, analyzed with this method, gives a similar field amplitude (within the error bars): $\sqrt{\langle E^2\rangle}=14.5\pm2.5$ kV/cm.

In the other method, the typical amplitude and frequency of the fields are determined by comparing the line experimental Fourier transform (from which the thermal contributions were subtracted) to the contribution of a single oscillatory field to the AF. The calculated results that fit best the experimental AF's are obtained with a field amplitude of $\simeq14$ kV/cm (in agreement with the value obtained by the previous method) and with a frequency of $(3-6)\times10^{11}$ Hz, close to the plasma electron frequency $\omega_{\rm pe}\simeq6\times10^{11}$ Hz.

The turbulent fields observed in this experiment are probably Langmuir waves excited as a result of a self-consistent generation of fast electrons in the POS. These electrons are generated by a voltage drop resulting from current-driven instabilities [39,40], that either cause the formation of a cathode sheath or give rise to anomalous resistivity. However, spatially resolved measurements of the electric field are highly required in order to study the effect of the current distribution in the POS on the evolution of the instability.

Because of their high frequency, the Langmuir oscillations do not give rise to anomalous momentum transfer from the electrons to the ions. As a result they have a negligible effect on the current distribution in the plasma, on the ion velocities, and consequently on the POS operation. Analysis of the line profiles also enabled us to obtain an upper limit for the amplitude of the low-frequency (ion acoustic) fluctuations in the plasma, found to be less than predicted by theoretical studies [7,53]. We estimated the resultant electron-ion collisionality due to these possible low-frequency waves and found it to be too low to cause the anomalous magnetic-field diffusion or the widening of the current channel that were observed in the experiment [20,19].

ACKNOWLEDGMENTS

The authors are grateful to H. Griem for his enlightening remarks, to A. Fruchtman for valuable discussions, and to E. Stambulchik for his help in the atomic physics calculations. This work was supported in part by the Minerva Foundation, Munich, Germany, and by the Israeli Academy of Science.

APPENDIX

Consider a line i subjected to the linear Stark effect due to either a thermal or nonthermal electric field. For short times, the AF, defined in Sec. IV, is correctly reproduced within the quasistatic approximation, and expressed as a sum over the Stark shifted components, i.e.,

$$C^i(t)=\sum_{k=0}^{N_i} L_k^i C_k(t), \tag{A1}$$

$$C_k(t)=\int dE\, W(E)\cos(ksEt), \tag{A2}$$

where $W(E)$ is the PDF of the electric field (E), $x=sEt$ is the linear Stark shift with $s=1.5(ea_0/\hbar)$ (e is the electron charge and a_0 is the Bohr radius), and L_k are numerical coefficients satisfying $\Sigma_{k=0}^{N_i} L_k^i=1$. The AF's for the H_α and H_β lines are [54]:

$$\begin{aligned} C^\alpha(t)=\int dE\, W(E)\frac{1}{14145}[&5490+3872\cos(x)\\ &+729\cos(2x)+2304\cos(3x)+1681(4x)\\ &+32\cos(5x)+36\cos(6x)+\cos(8x)], \end{aligned} \tag{A3}$$

$$\begin{aligned} C^\beta(t)=\int dE\, W(E)\frac{1}{2508}[&153\cos(2x)+912\cos(4x)\\ &+669\cos(6x)+384\cos(8x)+373\cos(10x)\\ &+16\cos(12x)+\cos(14x)]. \end{aligned} \tag{A4}$$

Unlike the thermal case, where for high fields $W(E)\propto E^{-5/2}$ [21], $W(E)$ is believed to have a Gaussian behavior in the nonthermal case [17,33]. However, in our analysis we make no assumption about the precise form of $W(E)$. The only requirement is that $W(E)$ drop fast enough for large fields so that $\langle E^2\rangle=\int_0^\infty dE\, W(E)E^2$ is finite. In that case, for short enough times, $\cos(ax)\simeq 1-(a^2x^2/2)$, and hence

$$\begin{aligned} C^\alpha(t)&=1-2s^2t^2\langle E^2\rangle,\\ C^\beta(t)&=1-\frac{62}{3}s^2t^2\langle E^2\rangle. \end{aligned} \tag{A5}$$

Thus if the Doppler and the thermal Stark broadening can be neglected, i.e., if $W(E)$ is purely due to nonthermal electric fields, then for short enough times $C(t)$ is quadratic in time.

We now turn to the case of both thermal and nonthermal Stark broadening, in which the resulting AF is a product of the AF's of the two contributions. We assume that the PDF of the thermal electric fields is given by the Holtsmark PDF [21,55]

$$W_H(E)=\frac{2E}{\pi E_H^2}\int_0^\infty x e^{-x^{3/2}}\sin\left(x\frac{E}{E_H}\right)dx, \tag{A6}$$

where

$$E_H=2\pi\left(\frac{4}{15}\right)^{2/3} e\sum_i (n_p Z_p^{3/2})^{2/3} \tag{A7}$$

is the Holtsmark Field, i.e., the field at the mean ion-ion distance (n_p and Z_p being the perturber density and charge, respectively). This is a very good approximation for our plasma parameters ($n_e\simeq 1\times 10^{14}$ cm^{-3} and $T_H\simeq T_e=2$ eV), resulting in less than a 10% difference from more exact calculations [56], and a much smaller difference in the strong field region (i.e., not near the line center) that is particularly important for our purposes. This approximation is convenient since the Holtsmark PDF gives analytic results for $C(t)$ [28].

By substituting $z\sin(zx)=-[d\cos(zx)/dx]$ in Eq. (A2) with $z=E/E_H$, integrating by parts over x and noting that the E-integral produces two δ functions, we obtain the thermal contribution:

$$\begin{aligned} C_k(t)&=\int_0^\infty \cos(a_kE)W_H(E)dE\\ &=e^{-(a_kE_H)^{3/2}}[1-\tfrac{3}{2}(a_kE_H)^{3/2}], \end{aligned} \tag{A8}$$

where $a_k=skt$.

For the evaluation of the nonthermal AF, let $P(E)$ denote the probability density for an electric field E to which the emitter is subjected. Assuming an isotropic $P(E)=W(E)/4\pi E^2$, one can show that

$$\begin{aligned} C_k(t)&=\int_0^\infty W(E)\cos(a_kE)dE\\ &=\int d^3\mathbf{E}P(\mathbf{E})e^{i\mathbf{a}_k\cdot\mathbf{E}}+i\int d^3\mathbf{E}P(\mathbf{E})\mathbf{a}_k\cdot\mathbf{E}e^{i\mathbf{a}_k\cdot\mathbf{E}}. \end{aligned} \tag{A9}$$

In the case of two isotropic and independent PDF's, labeled a and b, the total PDF is the convolution of the two PDF's:

$$P(\mathbf{E})=\int d^3\mathbf{E}_1 P_a(\mathbf{E}_1)P_b(\mathbf{E}-\mathbf{E}_1). \tag{A10}$$

Using Eqs. (A9) and (A10), and the convolution theorem, one obtains:

$$\begin{aligned} C_k(t)=C_{k,a}\int d^3\mathbf{E}_1 P_b(\mathbf{E}_1)e^{i\mathbf{a}_k\cdot\mathbf{E}_1}+\int d^3\mathbf{E}_1 P_a(\mathbf{E}_1)e^{i\mathbf{a}_k\cdot\mathbf{E}_1}\\ \times\left[C_{k,b}-\int d^3\mathbf{E}_2 P_b(\mathbf{E}_2)e^{i\mathbf{a}_k\cdot\mathbf{E}_2}\right]. \end{aligned} \tag{A11}$$

In our case a and b denote the nonthermal and thermal PDF's, respectively. It is known [21] for the thermal PDF

that $\int d^3\mathbf{E}\, P_b(\mathbf{E}_1) e^{i\mathbf{a}_k\cdot\mathbf{E}} = e^{-\overline{a}_k^{3/2}}$ where $\overline{a}_k = a_k E_H$. Using $C_{k,b}$ evaluated in Eq. (A8), we thus obtain

$$C_k(t) = e^{-\overline{a}_k^{3/2}}\left[C_{k,a} - \tfrac{3}{2}\overline{a}_k^{3/2} \int \mathbf{d}^3\mathbf{E}_1 P_a(\mathbf{E}_1) e^{i\mathbf{a}_k\cdot\mathbf{E}_1} \right]. \tag{A12}$$

For $a_k \to 0$ the integral approaches $1-(a_k^2/6)\langle E^2\rangle + O(a_k^4)$, where $\langle E^2\rangle$ is the average of E^2 over the nonthermal PDF. The result is that, as $t\to 0$,

$$C_k(t) \to 1 - \frac{5}{2}\overline{a}_k^{3/2} - \langle E^2\rangle \frac{a_k^2}{2} + 2\overline{a}_k^3 + O(\overline{a}_k^{7/2}). \tag{A13}$$

Multiplying the thermal and nonthermal AF's expanded according to Eq. (A1), using the nonthermal AF expansion in a way similar to that used in obtaining Eq. (A5), and using the thermal AF from the Taylor expansion of Eq. (A8) for each term, yields

$$\begin{aligned} C_a(t)C_b(t) &= \sum_\mu L_\mu \left(1 - \langle E^2\rangle \frac{a_\mu^2}{2} + \cdots\right) \sum_k L_k \left(1 - \frac{5}{2}\overline{a}_k^{3/2} + 2\overline{a}_k^3 + \cdots\right) \\ &= \sum_{k,\mu} L_k L_\mu \left(1 - \frac{5}{2}\overline{a}_k^{3/2} - \langle E^2\rangle \frac{a_\mu^2}{2} + 2\overline{a}_k^3 + \cdots\right) \\ &= 1 - \sum_k L_k \left(\frac{5}{2}\overline{a}_k^{3/2} + 2\overline{a}_k^3\right) - \sum_\mu L_\mu \langle E^2\rangle \frac{a_\mu^2}{2} + \cdots = C(t), \end{aligned} \tag{A14}$$

where $C(t)$ is the sum over the $C_k(t)$'s obtained in Eq. (A13). Thus, the total Stark AF is the product of the thermal and nonthermal AF's.

For short times, the Doppler contribution results in multiplying the Stark $C(t)$ by a term quadratic in time. This results in a total AF decaying in time:

$$C(t) = 1 - \sum_k L_k \left[\frac{5}{2}(ksE_H t)^{3/2} + \frac{t^2}{2}\left(k^2 s^2 \langle E^2\rangle + \frac{k_B T \omega_0^2}{Mc^2} \right) + O(t^3) \right], \tag{A15}$$

where M is the emitter mass, T is the Doppler temperature, ω_0 is the unperturbed frequency, and c is the speed of light.

At very short times there is also a linear-in-time contribution to $C(t)$ resulting from the impact contribution [21]. For hydrogenic lines, the most important contribution to the linear term is the ion impact which dominates the electron impact. However, the electron impact is applicable over times significantly longer than the ionic ones, which gradually changes to a power-law decay. In our case we have verified that over the times used to determine $\langle E^2\rangle$, both contributions are negligible compared to the quadratic term.

If the electric field in the plasma is directional, this treatment can also account for the polarization of the emitted spectra. Since the different k's in Eq. (A15) are polarized along the electric field (π components) or perpendicular to the field (σ components), summing over the appropriate terms will yield the $C(t)$ of light polarized in each direction. We also note that a similar treatment for non-hydrogen-like ions that experience a quadratic Stark effect yields the value of $\langle E^4\rangle$.

[1] C. W. Mendel and S. A. Goldstein, J. Appl. Phys. **48**, 1004 (1977).

[2] R. A. Meger, R. J. Commisso, G. Cooperstein, and Shyke Goldstein, Appl. Phys. Lett. **42**, 943 (1983).

[3] R. J. Commisso, J. P. Apruzese, D. Mosher, G. G. Peterson, S. J. Stephanakis, J. W. Thornhill, F. C. Young, and B. V. Weber, Bull. Am. Phys. Soc. **41**, 1423 (1996).

[4] B. M. Kovalchuk and G. A. Mesyats, Dokl. Akad. Nauk SSSR **284**(4), 857 (1985) [Sov. Phys. Dokl. **284**, 857 (1985)].

[5] IEEE Trans. Plasma Sci. **PS-15**, 629 (1987), special issue on fast opening vacuum switches, edited by G. Cooperstein and P. F. Ottinger.

[6] R. J. Commisso, G. Cooperstein, R. A. Meger, J. M. Neri, and P. F. Ottinger, in *Opening Switches*, edited by A. Guenther, M. Kristiansen, and T. Martin (Plenum, New York, 1987), pp. 149–175.

[7] R. M. Kulsrud, P. F. Ottinger and J. M. Grossmann, Phys. Fluids **31**, 1741 (1988).

[8] J. M. Grossmann, P. F. Ottinger, J. M. Neri, and A. T. Dorbot, Phys. Fluids **29**, 2724 (1986); J. M. Grossmann, P. F. Ottinger, and R. J. Mason, J. Appl. Phys. **66**, 2307 (1989).

[9] R. J. Mason, J. M. Wallace, J. M. Grossmann, and P. F. Ottinger, IEEE Trans. Plasma Sci. **PS-15**, 715 (1987); R. J. Mason and M. E. Jones, Phys. Rev. Lett. **61**(16), 1835 (1988).

[10] A. Kingsep, Yu. V. Mochov, and K. V. Chukbar, Fiz. Plazmy **10**, 854 (1984) [Sov. J. Plasma Phys. **10**, 495 (1984)]; A. Fruchtman, Phys. Fluids B **3**, 1908 (1991); K. Gomberoff and A. Fruchtman, *ibid.* **5**, 2841 (1993).

[11] A. V. Gordeev, A. V. Grechinkha, Ya. L. Kalda, A. V. Gulin, and O. M. Drozdova, Fiz. Plazmy **16**, 95 (1990) [Sov. J. Plasma Phys. **16**, 95 (1990)].

[12] J. M. Grossmann, C. R. DeVore, and P. F. Ottinger, in *Proceedings of the 9th International Conference on High Power Particle Beams*, Washington D.C., 1992 (National Technical Informational Service, Springfield, VA, 1992), Vol. 1, p. 559.
[13] A. S. Kingsep and A. Munier, J. Plasma Phys. **57**, 501 (1997).
[14] Yu. P. Golovanov, G. I. Dolgacgev, L. P. Zakatov, Yu. G. Kalinin, I. V. Piniskaya, A. G. Vehakov, and R. V. Chikin, Fiz. Plazmy **17**, 799 (1991) [Sov. J. Plasma Phys. **17**, 466 (1991)].
[15] G. I. Dolgachev, L. P. Zakatov, Yu. G. Kalinin, A. S. Kingsep, M. S. Nitishinski, A. G. Ushakov, Fiz. Plazmy **22**, 1017 (1996) [Plasma Phys. Rep. **22**, 921 (1996)].
[16] M. Baranger and B. Mozer, Phys. Rev. **123**, 25 (1961).
[17] G. V. Sholin and E. A. Oks, Dokl. Akad. Nauk SSSR **209**, 1318 (1973) [Sov. Phys. Dokl. **18**, 254 (1973)]; E. A. Oks and G. V. Sholin, Zh. Tekh. Fiz. **46**, 254 (1976) [Sov. Phys. Tech. Phys. **21**, 144 (1976)].
[18] S. Alexiou, A. Weingarten, Y. Maron, M. Sarfaty, and Ya. E. Krasik, Phys. Rev. Lett. **75**, 3126 (1995).
[19] M. Sarfaty, Y. Maron, Ya. E. Krasik, A. Weingarten, R. Arad, R. Shpitalnik, A. Fruchtman, and S. Alexiou, Phys. Plasmas **2**, 2122 (1995).
[20] R. Shpitalnik, A. Weingarten, K. Gomberoff, Ya. E. Krasik, and Y. Maron, Phys. Plasmas **5**, 792 (1998).
[21] H. R. Griem, *Plasma Spectroscopy* (McGraw-Hill, New York, 1964); *Spectral Line Broadening in Plasmas* (Academic, New York, 1974).
[22] J. Seidel, in *Spectral Line Shapes Vol. 6*, edited by L. Frommhold and J. Keto, AIP Conf. Proc. No. 216 (AIP, New York, 1990).
[23] E. W. Smith, J. Cooper, and C. R. Vidal, Phys. Rev. **185**, 140 (1969).
[24] *Atomic Data for Fusion*, edited by C. F. Barnett (Oak Ridge National Laboratory, Oak Ridge, TN, 1990), Vol. I (copies available from NIST, U.S. Department of Commerce, 5285 Port Royal Road., Springfield, VA 22161).
[25] S. Alexiou, Phys. Rev. A **49**, 106 (1994).
[26] E. W. Smith and C. F. Hooper Jr., Phys. Rev. **157**, 126 (1967); E. W. Smith, *ibid.* **166**, 102 (1968); D. Voslamber, Z. Naturforsch. **24A**, 1458 (1969).
[27] R. Stamm and D. Voslamber, J. Quant. Spectrosc. Radiat. Transf. **22**, 599 (1979); R. Stamm, E. W. Smith, and B. Talin, Phys. Rev. A **30**, 2039 (1984); R. Stamm, Y. Botzanowski, V. P. Kaftandjian, and B. Talin, Phys. Rev. Lett. **52**, 2217 (1984); F. Khelfaoui, A. Calisti, R. Stamm, and B. Talin, in *Spectral Line Shapes Vol. 6* (Ref. [22]).
[28] R. Stamm, B. Talin, E. L. Pollock, and C. A. Iglesias, Phys. Rev. A **34**, 4144 (1986).
[29] G. C. Hegerfeldt and V. Kesting, Phys. Rev. A **37**, 1488 (1988).
[30] T. J. Nee and H. R. Griem, Phys. Rev. A **14**, 1853 (1976); T. J. Nee, J. Quant. Spectrosc. Radiat. Transf. **38**, 213 (1987).
[31] E. A. Oks, *Plasma Spectroscopy: The Influence of Microwave and Laser Fields* (Springer, Berlin, 1995).
[32] H. J. Kunze and H. R. Griem, Phys. Rev. Lett. **21**, 1048 (1968).
[33] C. Deutsch and G. Bekefi, Phys. Rev. A **14**, 854 (1976).
[34] Y. Maron, E. Sarid, O. Zahavi, L. Perlmutter, and M. Sarfaty, Phys. Rev. A **39**, 5842 (1989).
[35] P. A. Robinson and D. L. Newman, Phys. Fluids B **2**, 3120 (1990).
[36] S. Alexiou, J. Quant. Spectrosc. Radiat. Transf. **54**, 1 (1995).
[37] M. A. Gigosos, J. Fraile, and F. Torres, Phys. Rev. A **31**, 3509 (1985); M. A. Gigosos, V. Cardenoso, and F. Torres, J. Phys. B **19**, 3027 (1986); V. Cardenoso and M. A. Gigosos, Phys. Rev. A **39**, 5258 (1989).
[38] S. Alexiou, Phys. Rev. Lett. **76**, 1836 (1996).
[39] V. D. Shafranov, in *Reviews of Plasma Physics*, edited by M. A. Leontovich (Consultants Bureau, New York, 1967), Vol. 3, pp. 1–158.
[40] A. B. Mikhailovskii, *Theory of Plasma Instabilities* (Consultants Bureau, New York, 1974), Vol. 1.
[41] A. A. Vedenov and D. D. Ryutov, in *Reviews of Plasma Physics*, edited by M. A. Leontovich (Consultants Bureau, New York, 1975), Vol. 6, pp. 1–76.
[42] J. L. Kalda and A. S. Kingsep, Fiz. Plazmy **15**, 981 (1989) [Sov. J. Plasma Phys. **15**, 568 (1989)].
[43] A. S. Kingsep and A. A. Sevastyanov, Fiz. Plazmy **17**, 1183 (1991) [Sov. J. Plasma Phys. **17**, 685 (1991)].
[44] R. J. Commisso, P. J. Goodrich, J. M. Grossmann, D. D. Hinshelwood, P. F. Ottinger, and B. V. Weber, Phys. Fluids B **4**, 2368 (1992).
[45] P. F. Ottinger, S. A. Goldstein, and R. A. Meger, J. Appl. Phys. **56**, 774 (1984).
[46] J. M. Grossmann, S. B. Swanekamp, P. F. Ottinger, R. J. Commisso, D. D. Hinshelwood, and B. V. Weber, Phys. Plasmas **2**, 299 (1995).
[47] A. Fruchtman, Phys. Plasmas **3**, 3111 (1996).
[48] A. A. Galeev and R. Z. Sagdeev, in *Reviews of Plasma Physics*, edited by M. A. Leontovich (Consultants Bureau, New York, 1979), Vol. 7, pp. 1–180.
[49] A. S. Kingsep, Fiz. Plazmy **17**, 582 (1991) [Sov. J. Plasma Phys. **17**, 342 (1991)].
[50] L. I. Rudakov and L. V. Korablev, Zh. Éksp. Teor. Fiz. **50**, 220 (1966) [Sov. Phys. JETP **23**, 145 (1965)].
[51] A. S. Kingsep, K. V. Chukbar, V. V. Yan'kov, in *Reviews of Plasma Physics*, edited by B. B. Kadomtsev (Consultants Bureau, New York, 1990), Vol. 17.
[52] A. S. Kingsep and A. A. Sevastyanov, Fiz. Plazmy **17**, 205 (1991) [Sov. J. Plasma Phys. **17**, 119 (1991)].
[53] R. N. Sudan and P. L. Similon, in *Proceedings of the 7th International Conference on High Power Particle Beams*, Karlsruhe, Germany, 1988, (Kernforschungszentrum Karlsruhe Gmbh, Karlsruhe, Germany, 1988), Vol. 1, p. 416.
[54] E. Schrödinger, Ann. Phys. (Leipzig) **80**, 457 (1926).
[55] J. Holtsmark, Ann. Phys. (Leipzig) **58**, 577 (1919).
[56] C. A. Iglesias, H. E. Dewitt, J. L. Lebowitz, D. MacGowan, and W. B. Hubbard, Phys. Rev. A **31**, 1698 (1985).